

Nature of the many-particle potential in the monatomic liquid state: Energetics, kinetics, and stability

D. C. Wallace and B. E. Clements

Theoretical Division, Los Alamos National Laboratory, Los Alamos, New Mexico 87545

(Received 9 September 1998)

Molecular-dynamics calculations have been used to explore and characterize the many-particle potential underlying the motion of particles in the monatomic liquid state. The potential used accurately represents metallic sodium at the density of the liquid at melt. It is found that the potential surface is composed of a large number of stable nearly harmonic valleys, and that these can be classified as random, symmetric, or crystalline. The random valleys cover by far the major portion of configuration space; they are macroscopically uniform, i.e., they all have the same structural potential and vibrational spectrum; and they all have microscopically irregular anharmonicity. The symmetric valleys lie at potential energies below the random valleys, but above the bcc crystalline valley. The symmetric valleys are not macroscopically uniform, but show scatter in their structural potentials and their eigenvalue spectra, and the symmetric valleys also have microscopically irregular anharmonicity. The equilibrium states of our system, from zero temperature up to and including the liquid states, fall into three groups, random, symmetric, and crystalline, according to which class of potential valley is mainly visited in the system motion. The random states are well separated from the symmetric and crystalline states, on the graph of mean potential energy versus temperature. The random states lie on a single line over the entire temperature range, and they include the liquid states, demonstrating that the random valleys dominate the statistical mechanics of the liquid. The present results provide detailed confirmation of the liquid-dynamics Hamiltonian previously used in equilibrium and nonequilibrium calculations. Further, the liquid-dynamics prediction of near equality of the log moment of the vibrational spectra, for the liquid and crystal at the same density, is verified here for the example of sodium. [S1063-651X(99)01903-0]

PACS number(s): 61.20.Ne, 61.20.Ja, 61.20.Gy

I. INTRODUCTION

The objective of this work is to characterize the many-particle potential underlying the motion of particles in the classical monatomic liquid state. Our technique is to analyze molecular-dynamics (MD) calculations for a comprehensive set of stable and metastable equilibrium states, from zero temperature up to and including the liquid, for a fixed density and a fixed interatomic potential. From the theory of liquid dynamics [1], one expects certain properties of the potential surface to be universal for monatomic systems, and these expectations will guide us in formulating an investigative strategy.

In liquid-dynamics theory [1], it is observed that the measured ion-motional specific heat is very nearly $3k_B$ per ion, for all classical monatomic liquids at melt. From this we assume that the ions move primarily within one or more nearly harmonic valleys in the potential surface. (A valley in this $3N$ -dimensional space is our generic term for the neighborhood of a local minimum in the many-body potential surface, about which the potential increases in all $3N$ directions.) It is also observed that the measured constant-volume entropy of melting, for normal melting elements [2], is very nearly a universal constant value $k_B\Delta$ per ion, where $\Delta = 0.80$. To interpret this entropy of melting, we need two results from statistical mechanics: first, the ions in the crystal move entirely within a single nearly harmonic valley in the potential surface, and second, the classical entropy per ion representing one harmonic valley is $3k_B[\ln(T/\Theta_0)+1]$, where T is the temperature, and Θ_0 is the characteristic temperature

determined by the logarithmic moment of the vibrational frequencies (defined in Sec. III). The universal entropy of melting then leads us to conclude (a) that the number of potential valleys accessible to the liquid is w^N , for N particles, where $\ln w = \Delta$, and (b), the characteristic temperatures Θ_0 are nearly the same for the crystal and the liquid valleys.

In a real monatomic liquid, the physical particles are approximately rigid ion cores, which we call simply “the ions.” The stable equilibrium configuration of ions at the bottom of a stable many-particle potential valley is called a “structure.” Molecular-dynamic calculations have given us much information about structures in model systems. From the pioneering work of Stillinger and Weber, we know that amorphous structures exist [3,4], and that their potential energies lie in a band above the crystalline potential energy [5–7]. LaViolette and Stump [8] found a wide variety of structure symmetries, depending on the interatomic potential and the density. These authors denoted noncrystalline structures by the general term “amorphous.” In considering the motion of ions in monatomic liquids, it became obvious that one had to subdivide the amorphous structures into two classes, with different expected properties, as follows [1].

First, structures with a remnant of crystal symmetry, at least among nearest neighbors, are called “symmetric” structures. The members of this class, though large in number, are still *relatively* few, because of the symmetry restriction. Also, since the structure potential [defined in Eq. (3.9) below] and vibrational frequencies are sensitive to near-neighbor symmetry, the macroscopic averages of these properties will show significant variations over the class of symmetric structures.

Second, structures with highly random near-neighbor orientations are called “random” structures, and their very randomness implies properties in contrast with symmetric structures. First, for large N , random structures constitute the great majority of all the structures, hence they dominate the statistical mechanics of the liquid state. Second, again for large N , each macroscopic average property is narrowly distributed over the class of random structures, i.e., the random structures are macroscopically uniform.

Another property of the potential surface often investigated by MD calculations is the set of instantaneous normal modes. These are the eigenvalues and eigenvectors of the potential energy curvature tensor, evaluated at the instantaneous configuration of the system, as it moves in an equilibrium state. The set contains a temperature-dependent lobe of negative eigenvalues, called the “unstable” modes. Rahman, Mandell, and McTague [9] estimated the spectrum for an amorphous system. LaViolette and Stillinger [10] showed that the mean number of negative eigenvalues increases strongly with temperature for the crystal, and continues to increase after melting to the liquid. Here, since we expect each valley to be nearly harmonic [1], our primary measure of the potential surface will be the set of ordinary (stable) normal modes evaluated at the valley bottom (at the structure). Beyond this harmonic measure, as we find in Sec. III, the number of negative eigenvalues among the instantaneous normal modes becomes an indicator of the nature of anharmonicity in the potential surface of a single valley.

We have chosen to work with an interatomic potential that accurately represents metallic sodium. This allows us to state unambiguously that the properties discussed in this work are realistic and not an artifact of the form of the chosen potential. For N atoms in a volume V , the positions of the ions are \mathbf{r}_K , for $K=1, \dots, N$, and in pseudopotential perturbation theory, applicable to nearly-free-electron metals, the total potential Φ takes the form [11,12]

$$\Phi(\{\mathbf{r}_K\}) = \Omega(V) + \frac{1}{2} \sum_{K,L} \phi(|\mathbf{r}_K - \mathbf{r}_L|; V). \quad (1.1)$$

$\Omega(V)$ is a large negative potential, which accounts for most of the metallic binding, and $\phi(r; V)$ is an effective ion-ion potential, which works through the screening electrons. We will fix the volume per atom $V_A = V/N$ at the value $278a_0^3$, which is the volume of liquid sodium at the melting temperature $T_m = 371$ K. At fixed V , $\Omega(V)$ is constant, so we choose the zero of energy here by setting $\Omega(V) = 0$. The original pair potential [13], given by pseudopotential theory, and calibrated to the bulk properties of crystalline sodium at $T = 0$, is shown in Fig. 1. This potential has long-range (Friedel) oscillations, but these give no significant contribution to the statistical mechanics of the liquid state. Therefore, to gain the numerical advantage of a short-range potential, we use a damped potential that smoothly removes the long-range oscillations. Our damped potential is obtained by multiplying the original potential by $\exp[-c(r-r_c)^2]$, where $c = 0.64a_0^{-2}$ and $r_c = 15.0a_0$, for all $r \geq 15a_0$. The damped potential is also shown in the inset in Fig. 1, and differs from the original potential only in the region of the Friedel oscillations, and only by a magnitude less than 10^{-5} Ry.

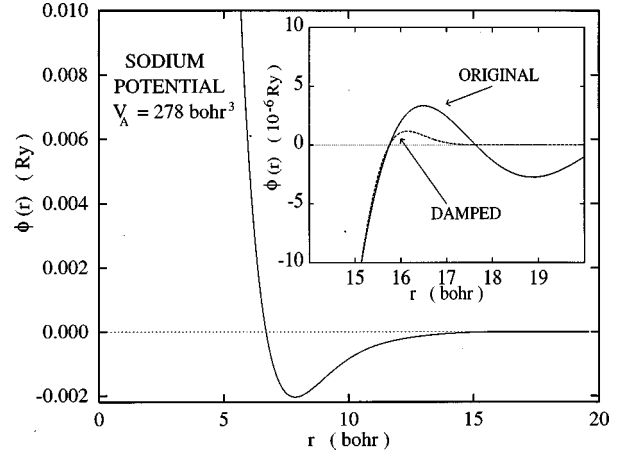


FIG. 1. The sodium potential $\phi(r)$ for $V_A = 278a_0^3$. The inset shows the pseudopotential form for the potential used in the work of Ref. [13] (ORIGINAL), which has Friedel oscillations at large r , and an exponentially damped version of the potential (DAMPED). The damped potential is used in our MD calculations.

The complete sodium potential in Eq. (1.1) has had remarkable success in accounting for the properties of metallic sodium. Excellent agreement with experiment was obtained for the phonon frequencies [13], for the temperature-dependent properties of the crystal [14,15], and of the liquid, [16], for properties of the crystal under pressure [17], and for the melting temperature as a function of pressure [18]. Hence, the damped pair potential used here will certainly yield physically realistic results for metallic sodium at $V_A = 278a_0^3$.

The calculations were carried out using the Verlet algorithm [19], for N particles in a cubical box, with periodic boundary conditions. We used $N = 168$ for exploratory calculations, $N = 432$ for bcc crystal calculations, and $N = 500, 1000$, and 3000 for final calculations on noncrystalline states. The MD time step is $\delta t = \sqrt{2Ma_0^3/e^2}$, where M is the atomic mass of sodium, or $\delta t = 7.00 \times 10^{-15}$ s. In the coming sections, it will be convenient to express the temporal evolution of certain physical quantities as a function of the MD iterations, rather than converting to units of time. The conversion factor is simply δt . A useful reference time in this study is the mean vibrational period of the particles. In all states we shall study, crystalline and noncrystalline alike, it is approximately $60\delta t$.

The system Hamiltonian is denoted

$$\mathcal{H} = \mathcal{K} + \Phi, \quad (1.2)$$

$$\mathcal{K} = \frac{1}{2} \sum_K M \mathbf{v}_K^2, \quad (1.3)$$

$$\Phi = \frac{1}{2} \sum_{K,L} \phi_{KL}, \quad (1.4)$$

where \mathbf{v}_K is the velocity of particle K , and $\phi_{KL} = \phi(|\mathbf{r}_K - \mathbf{r}_L|)$. During an MD run, $\mathcal{K}(t)$ and $\Phi(t)$ are fluctuating signals, with $\mathcal{K} + \Phi = \text{constant}$. When the system is in equilibrium, stable or metastable, the time average of a fluctuating quantity is a physically important measure. We de-

note the equilibrium time average of $F(t)$ by $\langle F(t) \rangle$, or simply $\langle F \rangle$ when the meaning is obvious. The equilibrium time average of the kinetic energy per particle is related to the temperature by

$$\langle \mathcal{K}/N \rangle = \frac{3}{2} k_B T. \quad (1.5)$$

In Sec. II, the equilibrium states of the system are found, and are classified into the two groups of random and symmetric, according to their mean potential energies as function of mean kinetic energy. It is shown that the localization of the system to a small region of configuration space is revealed in the mean square displacement as function of time. The properties of single potential valleys are examined in Sec. III, where it is found that both random and symmetric valleys are stable, that the random valleys have universal structure potential and eigenvalue spectrum, and that the small anharmonic potential is microscopically irregular in both random and symmetric valleys. In Sec. IV, the mean square displacement in equilibrium states is used to separate the motion into diffusive (intervalley) and nondiffusive (intra-valley) components. Our conclusions are summarized in Sec. V.

II. EQUILIBRIUM STATES OF THE SYSTEM

A. Generating the states

In the course of the MD calculations, we introduce special iterations for the purpose of cooling or heating the system. In one such iteration, each particle velocity is multiplied by a number ξ ,

$$\mathbf{v}_K \rightarrow \xi \mathbf{v}_K, \quad K=1, \dots, N. \quad (2.1)$$

The iteration is cooling when $0 \leq \xi < 1$, and heating when $\xi > 1$. When $\xi=1$, the iteration is called simply MD, and when this proceeds for an uninterrupted set of iterations it is called an MD run. If the heating or cooling iteration is sufficiently gentle, the system can be maintained near equilibrium, and for this condition we use $|\xi-1| < 10^{-3}$. The special case $\xi=0$ is called a quench. Repeated quenches move the system down the potential surface along the path of steepest descent.

Let us imagine that the many-particle potential surface is composed of a large number of intersecting valleys, and that the system in the liquid state moves very rapidly among these valleys. If we cool slowly from the liquid, so that the system remains near equilibrium, we expect the system, upon freezing, to settle into a special valley, namely, one as highly crystalline as possible, compatible with the periodic boundary conditions. On the other hand, a series of quenches will bring the system down within the valley it happens to be moving through when the quenches are initiated. Hence, quenching gives us the ability to make a statistical sampling of the valleys through which the system moves. If now the system is cold, and moves near the bottom of a particular valley, the system will remain in the same valley during a series of heating iterations, provided the heating is sufficiently gentle. Hence, heating gives us the ability to explore the potential surface of a single many-particle valley, at least up to its intersection with a neighboring valley.

Figure 2 shows representative curves of the system potential (energy) during a series of quenches from the liquid,

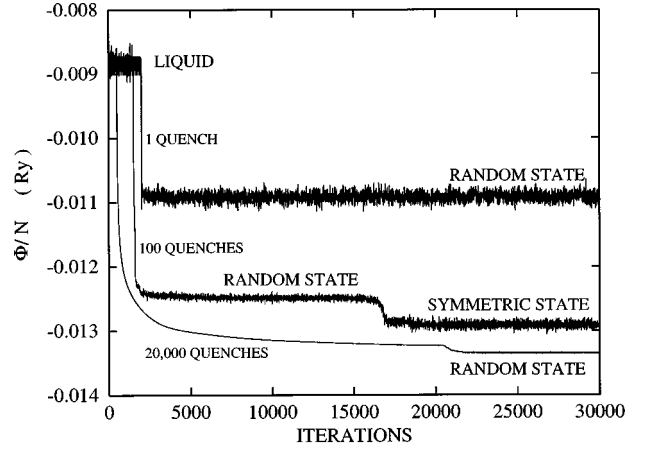


FIG. 2. The potential energy per particle as a function of MD iterations for 1, 100, and 20 000 quenches from the liquid state. The random state is short lived during the MD run containing 100 quenches. The final states reached, in all three runs, are long lived.

followed by MD runs. During the MD, the fluctuating potential initially decreases as the system gains kinetic energy, then it levels off and reaches equilibrium. Sometimes the system stays for awhile in one equilibrium state, then moves to another equilibrium state. This case is illustrated by the 100 quench run shown in Fig. 2. The state with the lower potential shall be referred to as the *lower* state. In nearly all the examples observed of a spontaneous change of state during an MD run, the system moved to a lower state (as illustrated in Fig. 2). It is convenient to make a qualitative separation of equilibrium states into “short-lived” states, which spontaneously decay, and “long-lived” states, which remain stable for as long as we choose to extend the MD calculations. The practical matter is that our ability to gather equilibrium data is limited by the lifetime of short-lived states, and hence our ultimate data for these states is less precise than for the long-lived states. In this work, we will investigate the properties of all the equilibrium states of the system, which we will call simply “states.” Mountain and Basu [20] made similar observations regarding potential energy plateaus and spontaneous transitions to lower-energy states (referred to as crystal nucleation in that work) for quenched Rb.

Most of the states we observed are metastable. If an original state spontaneously decays to a new state, during MD evolution, then the original state is metastable with respect to the new state. Absolute stability is much more difficult to establish, but for the present purposes it is not necessary to do so. Since it is useful to have available a set of crystalline states, for comparison with the amorphous states, we will apply our computational techniques to the crystalline bcc states at various temperatures. Then, among the states considered here, the stable ones are as follows: the bcc states for $T=0$ to around 350 K; a two-phase region from 350 to 371 K; and liquid above 371 K.

B. Energies of the states

States are characterized by the time-averaged potential and kinetic energies per particle, denoted, respectively, $\langle \Phi/N \rangle$ and $\langle \mathcal{K}/N \rangle$, where $\langle \mathcal{K}/N \rangle$ is equivalent to T by Eq. (1.5). For all the states we generated by one or more

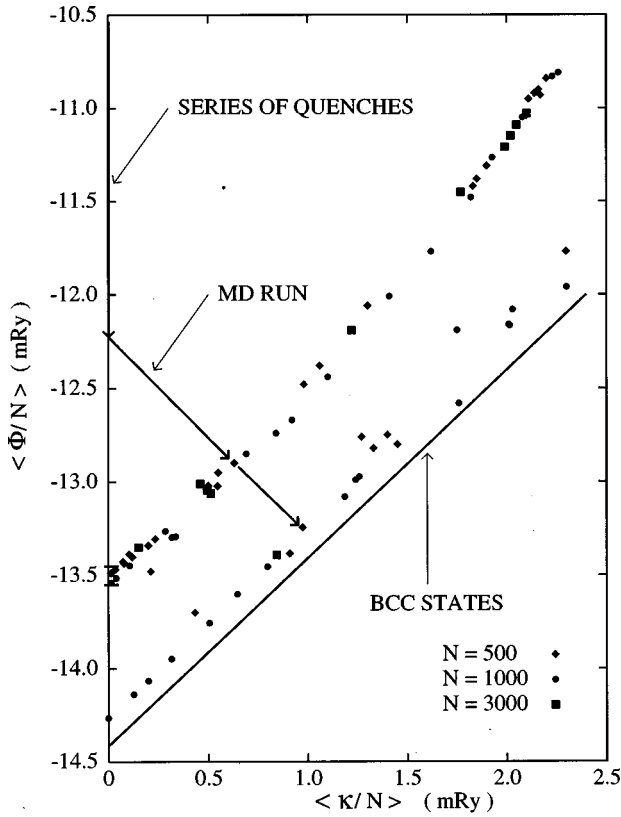


FIG. 3. $\langle \Phi/N \rangle$ vs $\langle \mathcal{K}/N \rangle$ for the random, symmetric, and bcc states. The small hatch marks on the $\langle \Phi/N \rangle$ axis show the spread $\langle \Phi/N \rangle$ obtained for 15 different valleys at $T \approx 0$.

quenches from the liquid state, for $N=500$, 1000, and 3000, $\langle \Phi/N \rangle$ is plotted versus $\langle \mathcal{K}/N \rangle$ in Fig. 3. The exception is that a number of very-low-temperature states are indicated merely by their range of $\langle \Phi/N \rangle$, since on this plot $\langle \mathcal{K}/N \rangle \approx 0$ for those states. A series of quenches moves the system down the $\langle \Phi/N \rangle$ axis, at $\langle \mathcal{K}/N \rangle = 0$. Then during the MD run, $\Phi + \mathcal{K}$ is constant, so a spontaneous change of state proceeds along a 45° line in Fig. 3. For illustration, the path is indicated for a calculation comprising 100 quenches from the liquid, followed by an MD run during which a spontaneous decay occurs. Figure 3 also shows the data for the bcc states.

In Fig. 3, the states reached by quenching from the liquid fall into clearly separated upper and lower groups. In Fig. 4, $\langle \Phi/N \rangle$ versus temperature T is plotted for states in the upper group, together with liquid states, and intermediate states obtained by cooling less than one full quench from the liquid. Since the data of Fig. 4 conform to a single curve, we will include all these states under the designation of the upper group. The significant properties we observed for the states in the upper and lower groups are as follows.

First, the upper group states lie on a single line for all N , with very little scatter (Fig. 4). Second, these upper group states are stable at high temperatures, being the liquid states, but are only metastable relative to the lower group at lower temperatures. Third, in the overwhelming majority of our calculations, following quenches from the liquid, the system first came into equilibrium in an upper state. Fourth, along the curve of Fig. 3, upper states satisfy the incremental rela-

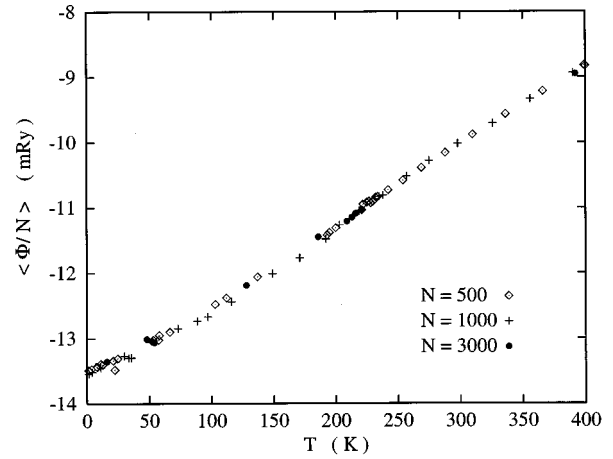


FIG. 4. $\langle \Phi/N \rangle$ vs the temperature T for the upper (random) states. The melting temperature for this potential is $T = 371$ K.

tion $\delta \langle \Phi/N \rangle \approx \delta \langle \mathcal{K}/N \rangle$, implying oscillations of the system within nearly harmonic many-particle valleys. Fifth, at the same mean kinetic energy, the lower group states have a much lower mean potential energy and show significant scatter about a single line (Fig. 3). Sixth, there is a temperature window $T_1 < T < T_2$, such that when the system arrives at an upper state for temperatures outside the window, it stays there, but when the system arrives at an upper state for temperatures within the window it subsequently transitions to a lower state. Our findings, for $N=500$, 1000, and 3000 are $T_1 \approx 35$ K and $T_2 \approx 200$ K. Noticeably different values of T_1 and T_2 might be found either for much longer MD runs, or for much larger systems, than were studied here. The short-lived upper group states within the window are often stable long enough to obtain respectable equilibrium data, say for 10^4 iterations.

We now provide an interpretation of these results which appears justified, in view of the conjectures of liquid dynamics theory (summarized in Sec. I). At the heart of this interpretation is the existence of the two classes of structures, random and symmetric [1].

For states in the upper group, the system moves primarily in random valleys, since this group has higher potential energy than the lower group, at the same kinetic energy (Fig. 3). Since the quenched liquid nearly always comes to equilibrium (short lived or long lived) in the upper group, the random valleys apparently cover the *majority* of configuration space sampled by the liquid. The continuity of the upper states with the liquid states (Fig. 4) suggests the random valleys dominate the statistical mechanics of the liquid. Finally, the random valleys are approximately harmonic.

For states in the lower group, the system moves primarily in symmetric valleys, where the remnant symmetry is responsible for lowering the potential relative to the upper group. In principle, symmetric states exist from the lower branch shown in Fig. 3, down to the crystal states. For example, microcrystalline bcc states should lie just slightly above the single-crystal bcc states shown in the graph. However, the complete range of symmetric states is not accessible in our calculations, due to limitations arising from the periodic boundary conditions and the small system size. Further, we cannot dismiss the possibility that symmetric states exist

that lie above the symmetric branch shown in Fig. 3, although they were never observed by us.

These interpretations are consistent with the conjectures of liquid-dynamics theory. Henceforth, we will refer to the upper group as the random states, and the lower group as the symmetric states. In the following paper we will use the calculated pair distribution functions, interatomic angular distributions, and other geometric measures among near-neighbors, to investigate the symmetry properties of the random and symmetric states.

C. Mean square displacement

In Sec. IV, the mean square displacement will provide a precise measure of the system motion in equilibrium states. Here, we want to use this function in a more qualitative way. For general nonequilibrium processes, the mean square displacement $d(t, t_0)$ is

$$d(t, t_0) = \frac{1}{6N} \sum_K [\mathbf{r}_K(t) - \mathbf{r}_K(t_0)]^2. \quad (2.2)$$

If for a period of time during an MD run, the system moves only within a fixed small region of configuration space, the fluctuating time signal $d(t, t_0)$ has a constant mean value during that period.

An example is shown in Fig. 5, where from the liquid state, a series of 800 quenches, followed by an MD run, was started at $t_0 = 0$. The kinetic and potential energies, as well as the mean square displacement, are shown for the same calculation. One can see the progress of the system energies during the quenches, during the approach to equilibrium, while the system is in an equilibrium state, and when it is moving between states. Exactly the same processes can be seen in the curve of $d(t, t_0)$ in Fig. 5. $d(t, t_0)$ adds two important pieces of information, however. First that in the equilibrium states achieved in Fig. 5, $d(t, t_0)$ maintains a constant mean, implying that the motion of the system is confined to a small region of configuration space, and second, when the system spontaneously transitions from one equilibrium state to another, it actually moves some distance in configuration space.

In Sec. III, we will concentrate on very-low-temperature states. A crucial property of these states, as revealed by their graphs of $d(t, t_0)$ versus time, is that they are confined to a very small region of configuration space. This is not a property of all equilibrium states, but of only a subset of them, as will be clarified in Sec. IV.

III. PROPERTIES OF THE MANY-PARTICLE POTENTIAL VALLEYS

A. Local dynamical matrix

We define the local dynamical matrix as the customary dynamical matrix from lattice dynamic theory, but evaluated at any point on the potential surface. The particles are labeled $K = 1, \dots, N$, Cartesian components are $i = x, y, z$, and the combined index K, i is $\beta = 1, \dots, 3N$. Cartesian components of the particle positions are r_β , and the second-order or harmonic potential coefficients at any spatial location are

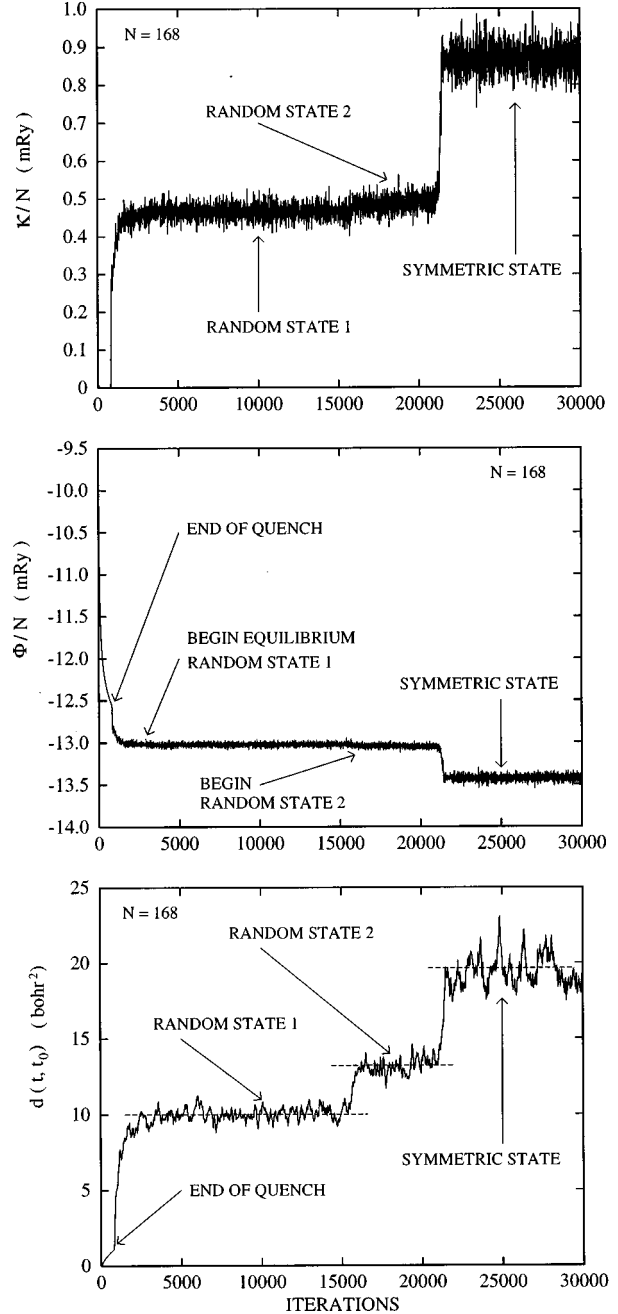


FIG. 5. The kinetic energy per particle (top), potential energy per particle (middle), and mean square displacement (bottom) for an $N=168$ particle system that was initiated by an 800 iteration quench from the liquid state.

$$D_{\beta\beta'} = \frac{\partial^2 \Phi}{\partial r_\beta \partial r_{\beta'}}. \quad (3.1)$$

The elements $D_{\beta\beta'}$ form the real symmetric $3N \times 3N$ local dynamical matrix, where ‘‘local’’ expresses the dependence on location. This matrix is diagonalized by a real orthogonal transformation, to yield the real eigenvalues $M \omega_\lambda^2$, for $\lambda = 1, \dots, 3N$. When the dynamical matrix is evaluated at a local potential minimum, as in lattice dynamics theory, the ω_λ are frequencies of the normal modes of vibration of

the N -particle system. In the more general case considered here, the local eigenvalues $M \omega_\lambda^2$ remain an important characteristic of the potential surface, since they measure the local curvature in $3N$ orthogonal directions.

For a translationally invariant system, three of the dynamical matrix eigenvalues represent uniform translation, and hence vanish. In our MD calculations, the three “zero” eigenvalues are more than 10 orders of magnitude smaller than the smallest of the remaining eigenvalues. The remaining $3N-3$ eigenvalues are called “nonzero,” and can be either positive or negative. When taking averages over the spectrum, the zero eigenvalues are always omitted. For example, the n th moment of the frequency distribution, denoted $\langle \omega^n \rangle$, is defined by

$$\langle \omega^n \rangle = \frac{1}{3N-3} \sum'_\lambda \omega_\lambda^n, \quad (3.2)$$

where \sum'_λ is over the $3N-3$ nonzero frequencies.

We now examine the many-particle potential surface within single valleys, hence it is necessary to eliminate the intervalley diffusive motion from the MD system. We do this by analyzing the system at a sufficiently low temperature that it moves entirely within a single valley. All the analysis of the present section is done for states where the system remains in a single valley during an MD run, and one by one, many different valleys are examined.

B. Stability of the random valleys

After repeated quenches from the liquid, the system arrives at a low-temperature long-lived random state. Following 20 000 quenches, and (very) long MD runs, for example, the system comes to equilibrium at approximately 10 K, and remains in this state for as long as we continue the MD run. Further, the mean square displacement tells us that the system is localized to a small region of configuration space. We suspect that the system is moving in a single random valley, and will prove this conjecture in Sec. IV. Meanwhile, we would like to determine whether or not this random valley is stable. Stability would be proved if we could move the system to the valley bottom, i.e., the equilibrium configuration where all forces vanish, and there evaluate the dynamical matrix, and find that all its eigenvalues are positive. Unfortunately, as long as we are limited to using numerical procedures, we can never place the system exactly at that configuration, hence we can never prove stability. We shall have to be satisfied with establishing a preponderance of numerical evidence for stability.

Figure 6 shows representative curves of the system potential Φ along a single normal coordinate q . An N -particle potential valley is stable if, and only if, the potential is stable in all $3N-3$ nontranslational normal coordinates. The potential in Fig. 6(a), has zero slope and zero curvature at q_0 , and is unstable. If our system contains such a potential in some direction, then under continued quenches and MD runs, two things will happen: First the system will eventually move off to the right, away from q_0 , and second, the system potential will decrease below Φ_0 , having no apparent lower bound. On the other hand, when a local measurement of the system eigenvalue is performed, this normal mode will yield a, re-

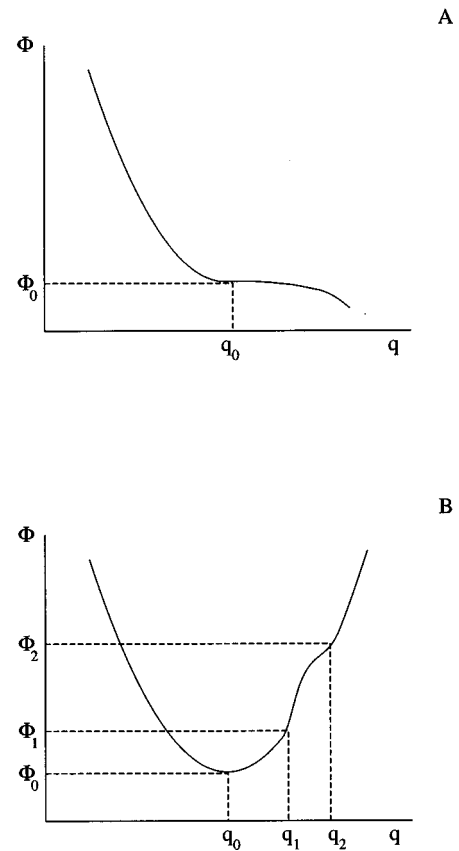


FIG. 6. Representative projections of the many-body potential Φ along a single normal coordinate q . The potential in A(B) illustrates the case of an unstable (stable) valley.

spectively, positive or negative eigenvalue, if the system is to the left or to the right of the equilibrium point q_0 . Next consider the potential curve shown in Fig. 6(b). It is stable, but the curve has inflection points at q_1 and q_2 , with negative curvature between q_1 and q_2 . If the system has energy below Φ_1 in this mode, a measurement of the local eigenvalue will always yield a positive result. If the system has energy between Φ_1 and Φ_2 in this mode, a measurement of the local eigenvalue will yield a positive or negative result, depending on whether the system is to the left or to the right of q_1 . Finally, if the system has energy greater than Φ_2 in this mode, the eigenvalue will be found sometimes positive and sometimes negative, but less often negative as the system energy increases above Φ_2 . In any case, once the system is trapped within this valley, then under continued quenches and MD runs it will remain in this valley, and while the energy can only decrease, it is bounded below by Φ_0 . Our conclusion from this discussion is (a) the system can exhibit all positive eigenvalues when it is in an unstable valley, (b) negative eigenvalues can appear for a stable valley, and (c) the strongest numerical evidence for stability is the freezing of the system location and energy, under continued quenches and MD runs.

Our procedure is to start with a random state, at say 10 K, and continue to cool with quenches, interspersed with MD runs, for a total on the order of 10^5 quenches and 10^5 to 10^6 MD iterations. During each MD run, the kinetic energy

equilibrates, so we can continue to use temperature to characterize the states reached.

We find the following results. The potential of the system converges towards a minimum value; upon continued quenching the *decrease* in the potential approaches a value that is essentially zero. Consistent with this, the mean square displacement demonstrates that the system remains confined to a small region in configuration space, and the lower the temperature, the smaller the region. These results hold without fail for every random state we studied ($N=500, 1000,$ and 3000). We conclude that the low-temperature random valleys are stable.

Some details of these calculations are of interest. First, upon quenching from the equilibrium liquid, the system always became trapped in a stable random valley, for $N=500, 1000,$ and 3000 . However, for one such run for the very small 168-particle system, during a series of quenches from the liquid, the system potential merely paused at the level of a random state, and then moved down to the level of a symmetric state. This result suggests that unstable random valleys might always be present, but will have no statistical significance except at very small N . Second, upon sampling the eigenvalue spectrum during MD runs, we do find negative eigenvalues, whose number decreases as the temperature decreases, and we find all positive eigenvalues below a certain temperature, for each valley. However, this alone is not strong evidence of stability, as noted in the discussion of Fig. 6. On the other hand, the fluctuations of the eigenvalues provide insight into the small-scale nature of the potential surface, as will be discussed shortly.

We made a set of accurate measurements for ten different random valleys, five each for 500- and 1000-particle systems. In each case, the minimum potential reached, and maintained throughout subsequent quenches and MD runs, is the static structure potential Φ_0 . For all the random valleys, Φ_0 lies in a very narrow range, with mean and variance given by

$$\Phi_0/N = -0.01352 \pm 0.00002 \text{ Ry/particle.} \quad (3.3)$$

We are not able to find any statistically meaningful N dependence in our data for Φ_0 , although in keeping with the prediction of liquid-dynamics theory, we presume the width of the Φ_0 distribution goes to zero as $N \rightarrow \infty$ [1].

C. Eigenvalue spectrum of the random valleys

Let us now inquire about the overall shape of the random valleys. This shape is measured in the harmonic (curvature) approximation by the eigenvalue spectrum. We therefore examine the eigenvalue spectrum calculated at well-separated instances during low-temperature MD runs, and for the present analysis, we take only examples where all eigenvalues are positive. This condition is satisfied by all the random states we studied, at temperatures of 10^{-3} K and below. The most notable property from the outset is that the overall eigenvalue spectrum for random valleys is universal. It is practically the same for different locations in a given valley; for different valleys; and for different N . The eigenvalue spectra for five different valleys are shown in Fig. 7. These spectra deviate from each other by an amount not more than the pen width of the drawn curves.

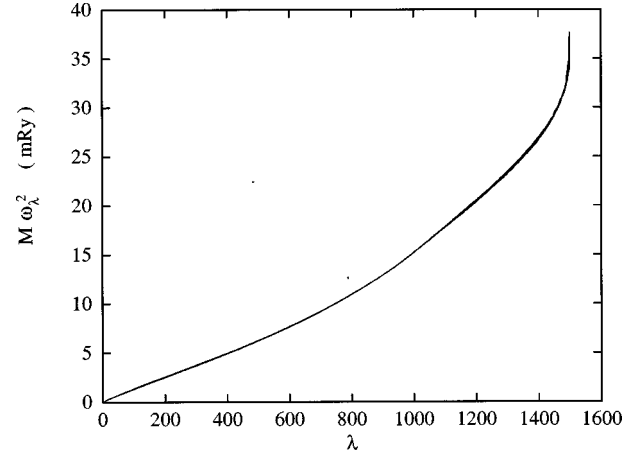


FIG. 7. Eigenvalues $M\omega_\lambda^2$, as a function of λ , for five different random valleys. These spectra were calculated at low temperatures (10^{-3} K or less) where all the eigenvalues are positive.

To obtain an approximate but simple representation of the complete eigenvalue spectrum, we will evaluate certain of its moments. In these terms, we can bring precision to our comparison of different random valleys. Three moments that have special importance in the classical statistical mechanics of harmonic valleys are the $-2, 0,$ and $+2$ moments of the frequency spectrum. These moments are expressed in terms of three characteristic temperatures $\Theta_n, n=-2,0,2,$ defined as follows:

$$k_B \Theta_{-2} = [\frac{1}{3} \langle (\hbar \omega)^{-2} \rangle]^{-1/2}, \quad (3.4)$$

$$\ln k_B \Theta_0 = \langle \ln \hbar \omega \rangle, \quad (3.5)$$

$$k_B \Theta_2 = [\frac{5}{3} \langle (\hbar \omega)^2 \rangle]^{1/2}, \quad (3.6)$$

where $\langle f(\omega) \rangle$ denotes an average of $f(\omega)$ over the frequency spectrum, as in Eq. (3.2). We note that Θ_{-2} is extremely sensitive to small variations in the lowest frequencies ω_λ , i.e., in the lowest dynamical-matrix eigenvalues $M\omega_\lambda^2$.

For 500- and 1000- particle systems, at temperatures of 10^{-3} K down to 10^{-6} K, we studied the fluctuations in Θ_n . The fluctuations as the system moves within a single random valley are quite small, while fluctuations from valley to valley are larger. We expect the intervalley fluctuations to approach zero as $N \rightarrow \infty$, and the statistics we have for $N=500$ and 1000 do support this expectation. For each of the central moments of the harmonic frequency spectrum, the mean and variance over our reference set of ten different random valleys, five each with $N=500$ and 1000 , are given by

$$\Theta_2 = 154.0 \pm 0.1 \text{ K}, \quad \Theta_0 = 98.7 \pm 0.1 \text{ K}, \quad (3.7)$$

$$\Theta_{-2} = 114 \pm 4 \text{ K}.$$

These results may be considered to represent a universal random valley, evaluated at the structure, i.e., at the valley bottom.

D. Negative eigenvalues and anharmonicity

Consider a stable valley the equilibrium configuration of which is given by the set of coordinates R_β , for $\beta = 1, \dots, 3N$. When the system is in this valley, the particle position coordinates r_β are conveniently expressed in terms of the displacements u_β , defined by

$$r_\beta = R_\beta + u_\beta. \quad (3.8)$$

Within the valley, the potential can be written

$$\Phi(\{r_\beta\}) = \Phi_0 + \Phi_H + \Phi_A, \quad (3.9)$$

where the structure potential is $\Phi_0 = \Phi(\{R_\beta\})$, the harmonic potential is

$$\Phi_H = \frac{1}{2} \sum_{\beta\beta'} \Phi_{\beta\beta'} u_\beta u_{\beta'}, \quad (3.10)$$

and the anharmonicity is expressed by Φ_A . The potential coefficients $\Phi_{\beta\beta'}$ constitute the dynamical matrix at equilibrium, and the transformation that diagonalizes this matrix puts Φ_H in the form

$$\Phi_H = \frac{1}{2} \sum_\lambda M \omega_\lambda^2 q_\lambda^2, \quad (3.11)$$

where each normal mode coordinate q_λ is a linear combination of the u_β .

Now consider our MD system, in equilibrium, moving only within this single stable valley, and suppose the anharmonicity is such that Φ has the shape shown in Fig. 6(b), for one or more of the normal coordinates q_λ . If the system is at very low temperature, the motion covers only a very small region near the valley bottom, and the eigenvalue, for this mode, is always positive. If the temperature is increased, the system moves over a larger portion of the valley surface, and we expect to find at first an occasional negative eigenvalue, then more negative eigenvalues, as the temperature continues to increase. This is indeed our qualitative finding, but the details are rather surprising.

Let n_- be the number of negative eigenvalues in a given calculation of the eigenvalue spectrum, and for an MD run with the system in an equilibrium state, let $\langle n_- \rangle$ be the average for a number of uncorrelated determinations of n_- . To remove the leading N dependence, we define the mean fraction of negative eigenvalues as

$$f_- = \frac{\langle n_- \rangle}{3N-3}. \quad (3.12)$$

Our results for random valleys are as follows. First, for a given random valley, negative eigenvalues begin to appear at very low temperature, in the range of 10^{-3} – 10^{-1} K, and the curve of f_- versus T is irregular, not a smooth curve. This irregular temperature dependence presumably results from a few small low-lying ‘‘bumps’’ in the potential curve, similar to that illustrated in Fig. 6(b). Second, at modest temperatures, of say 10 K or less, the f_- data are significantly different from one random valley to another. But for such temperatures, f_- is on the order of 10^{-3} or less, hence f_- measures a microscopic property of each valley, and such

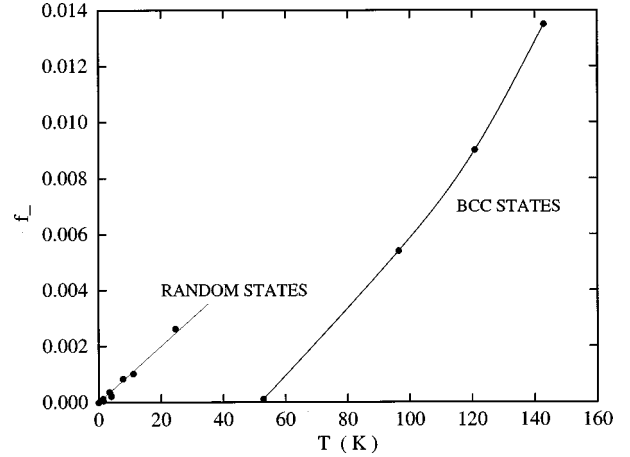


FIG. 8. The mean fraction of negative eigenvalues for low-temperature random states and for bcc states. The curves are for the purpose of guiding the eye.

a property should, by all means, vary from valley to valley. Hence the picture emerges that the anharmonic potential Φ_A for random valleys contains a contribution that is microscopically bumpy, and that varies from valley to valley. On the other hand, as T increases, and correspondingly f_- increases, a common trend begins to emerge for the random valleys. Our results for f_- versus T for two random valleys are graphed in Fig. 8.

A further perspective is gained by doing the same analysis for the bcc crystalline states. For our system, the bcc structure is stable, hence $n_- = 0$ for the bcc state at $T=0$. Upon heating the crystal to states at higher temperatures, f_- remains zero up to 52 K, but there f_- departs from zero, and increases as temperature continues to increase. The curve is shown in Fig. 8. The stability of the bcc valley can be appreciated from the fact that the bcc states remain stable in our MD calculations up to temperatures around 350 K. Hence, the bcc results provide an excellent example of the situation anticipated in our discussion of the stability of valleys, namely of the appearance of negative eigenvalues for a system moving in a single stable anharmonic valley. Further, the bcc curve of f_- versus T is smooth, suggesting Φ_A for the bcc crystal is a smooth function, in contrast to the microscopically bumpy character of Φ_A for the random valleys.

E. Crystal and symmetric valleys

Because we already have an extensive understanding of the bcc valley, the bcc states will often serve us as a reference point in our present work. For the system we are studying, accurate values of the harmonic parameters of the bcc potential valley are as follows:

$$\begin{aligned} \Phi_0 &= -0.014415 \text{ Ry}, & \Theta_2 &= 151.4 \text{ K}, \\ \Theta_0 &= 99.65 \text{ K}, & \Theta_{-2} &= 121.4 \text{ K}. \end{aligned} \quad (3.13)$$

These values are in accurate agreement with much earlier work on the lattice-dynamic properties of crystalline sodium [14,17].

Of the noncrystalline valleys we observed (random and symmetric), the random valleys are apparently the only sig-

nificant contributors to the liquid statistical mechanics, and for that reason we have placed major emphasis on uncovering the properties of the random valleys. Still, the symmetric valleys, through their contrasting properties, will help us to further understand the random valleys. In addition, the symmetric valleys are expected to have a role in the description of amorphous solids.

Though our investigation of symmetric valleys is far from exhaustive, the following properties are established. First, the symmetric valleys we have found are stable. Second, different symmetric valleys exhibit nominal differences in their macroscopic average properties, specifically in their values of Φ_0 and Θ_n for $n = -2, 0, 2$. This difference is in contrast to the accurate macroscopic uniformity of the random valleys. Finally, on increasing the temperature from very low values, negative eigenvalues begin to appear at rather low temperatures for symmetric valleys. From this we conclude that the symmetric valleys, like the random ones, have a microscopically bumpy anharmonic potential.

IV. DIFFUSIVE AND NONDIFFUSIVE MOTION

A. Diffusing states

In the last section, we studied the shape of the potential surface in stable anharmonic valleys. We now take the first step in studying the motion of the system, when it is confined to a single valley, and when it moves from valley to valley, in various equilibrium states. For this purpose, we study the mean square displacement, defined in Eq. (2.2).

For equilibrium states, $d(t, t_0)$ depends only on $t - t_0$, so we use the notation

$$d(t) = \frac{1}{6N} \sum_K [\mathbf{r}_K(t) - \mathbf{r}_K(0)]^2. \quad (4.1)$$

In general form, $d(t)$ increases from zero at $t = 0$, then fluctuates about linear dependence on t . The initial increase from zero is the ‘‘ballistic’’ regime, lasting less than half of a mean vibrational period. We fit the linear regime to a straight line $D_I + D_M t$, defining the intercept D_I and the slope D_M . In statistical mechanics, one shows [21] that D_M is the self-diffusion coefficient D . However, most of our states are metastable, hence they do not sample all of configuration space, so we use the subscript M to indicate that D_M measures the self diffusion only within a metastable state.

Figure 9 shows $d(t)$ for a set of random states, including the liquid. The curves show a uniform decrease in slope as temperature decreases. Our interpretation of Fig. 9 is that the system is moving among random valleys, for the liquid and random states alike, but the intervalley motion becomes slower as temperature decreases. This behavior is made more precise in Fig. 10, where D_M versus T is plotted for the random states shown in Fig. 9, plus several lower-temperature states. Figure 10 shows, by a different measure, the same property we observed in Fig. 4, that the entire collection of random *and* liquid states conform to a single temperature-dependent behavior.

States having $d(t)$ curves such as those shown in Fig. 9, with $D_M > 0$, are called diffusing states. From Fig. 10, the random states are diffusing states for $T \gtrsim 100$ K.

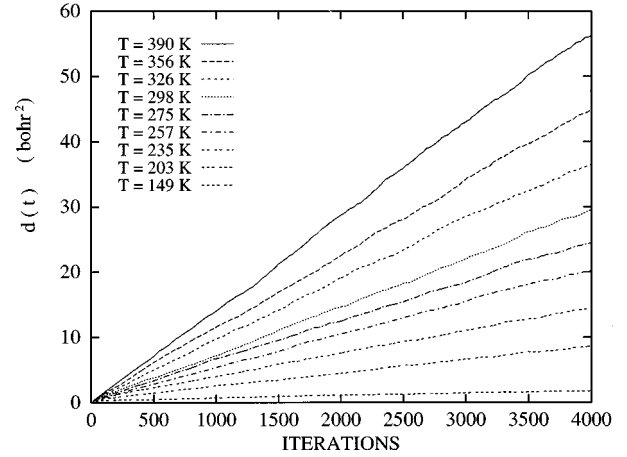


FIG. 9. The mean square displacement for the liquid state ($T = 390$ K), and for a set of diffusing random states ($149 \text{ K} \leq T \leq 356 \text{ K}$).

It is of interest to compare our calculation of D_M for the liquid state with the experimentally measured self-diffusion in liquid sodium. From a set of 11 calculations at $T = 401$ K, we find $D_M = 5.80 \pm 0.20 (10^{-5} \text{ cm}^2/\text{s})$. Experiment for liquid sodium at the same temperature and 1 bar pressure, where the actual volume is $280a_0^3/\text{atom}$, compared to our present volume of $278a_0^3/\text{atom}$, gives $D = 5.3 (10^{-5} \text{ cm}^2/\text{s})$ [22]. The discrepancy is in the range to be expected from combined errors of theory and experiment.

B. Nondiffusing states

At temperatures $T \lesssim 100$ K, the random states exhibit $D_M = 0$, at least to the accuracy available in our MD calculations. States with $D_M = 0$ are called nondiffusing states. Figure 11(a) shows $d(t)$ for a set of nondiffusing random states, while bcc states, for comparison, are shown in Fig. 11(b). In curves such as these, we fit $d(t)$, after its initial rise

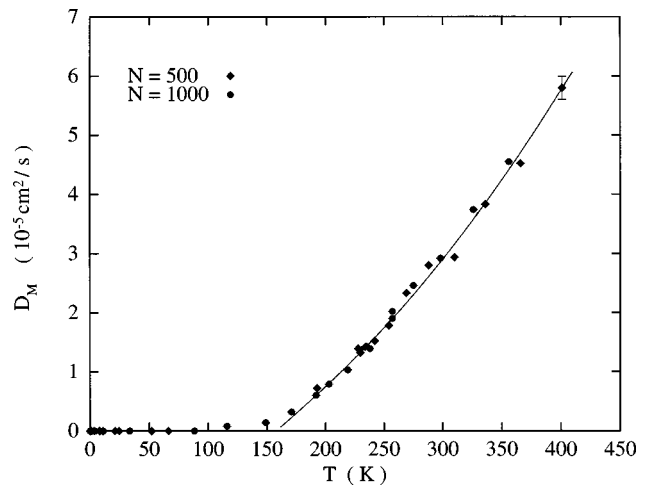


FIG. 10. Temperature dependence of the slope D_M , of the $d(t)$ curve for diffusing and nondiffusing ($D_M = 0$) random states as a function of temperature. The size of the error bar on the last data point is representative of the size of the uncertainty for all the diffusing states. Uncertainties in D_M for the nondiffusing states range from 10^{-3} at 100 K to 10^{-5} at 1 K, in the units graphed.

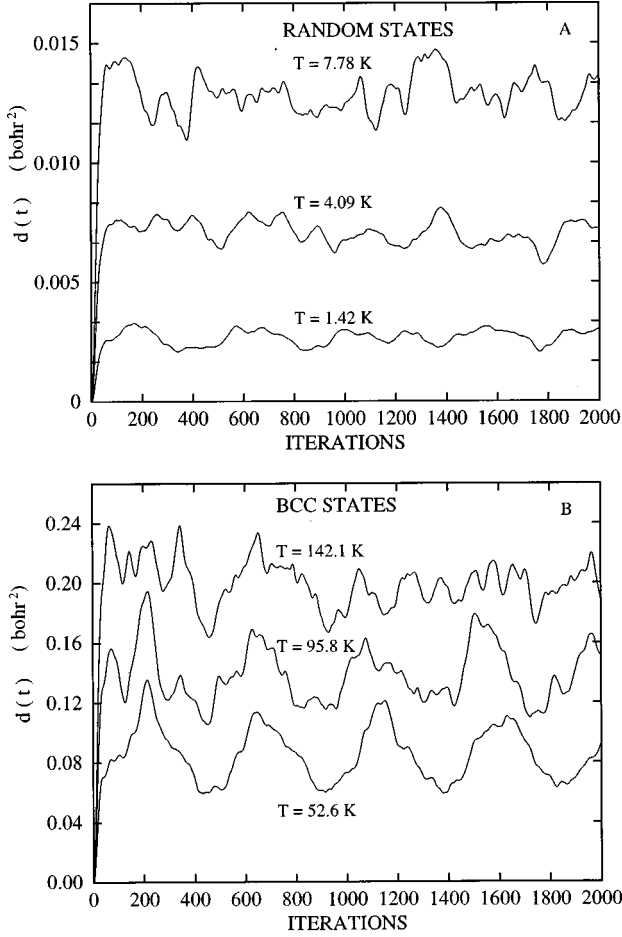


FIG. 11. The mean square displacement $d(t)$ for three nondiffusing random and bcc states.

from zero, to a horizontal line. From this line we get the intercept value, which for nondiffusing states is the long-time time average of $d(t)$:

$$D_I = \langle d(t) \rangle. \quad (4.2)$$

For completeness, on our graph of D_M versus T , the random states for which we observed $D_M=0$ are also indicated in Fig. 10.

The property $D_M=0$ tells us the system is trapped within some region of configuration space. In the present case, we suspect the system is trapped in a single valley in the potential energy surface. This hypothesis can be tested in the harmonic approximation, which should be quite accurate. For motion in a single valley, particle K has equilibrium position \mathbf{R}_K , and instantaneous position $\mathbf{r}_K(t) = \mathbf{R}_K + \mathbf{u}_K(t)$. Then $\langle d(t) \rangle$ is expressed from Eq. (4.1), and is evaluated as follows, for t beyond the ballistic regime.

$$\begin{aligned} \langle d(t) \rangle &= \frac{1}{6N} \left\langle \sum_K [\mathbf{r}_K(t) - \mathbf{r}_K(0)]^2 \right\rangle, \\ &= \frac{1}{6N} \left\langle \sum_K [\mathbf{u}_K(t) - \mathbf{u}_K(0)]^2 \right\rangle, \end{aligned}$$

$$= \frac{1}{6N} \left\langle \sum_K [\mathbf{u}_K^2(t) + \mathbf{u}_K^2(0)] \right\rangle, \quad (4.3)$$

where the last line follows because the cross terms $\mathbf{u}_K(t) \cdot \mathbf{u}_K(0)$ average to zero. Now if $N \rightarrow \infty$, the two sums become equal, so that at finite N they differ by a term of relative order N^{-1} , which we neglect, and thus

$$\langle d(t) \rangle = \frac{1}{3N} \left\langle \sum_K \mathbf{u}_K^2(t) \right\rangle. \quad (4.4)$$

Our system is constrained to zero center-of-mass motion, which means $\sum_K \mathbf{u}_K(t) = 0$. We indicate the constrained sum with a prime, as \sum'_K , and transform to normal coordinates, where \sum'_λ means to omit the three modes of uniform translation, having $\omega_\lambda = 0$. Then Eq. (4.4) becomes

$$\frac{1}{3N-3} \left\langle \sum'_K \mathbf{u}_K^2(t) \right\rangle = \frac{1}{3N-3} \left\langle \sum'_\lambda q_\lambda^2(t) \right\rangle. \quad (4.5)$$

With the system in equilibrium within a single harmonic valley, we have

$$\langle q_\lambda^2(t) \rangle = \frac{k_B T}{M \omega_\lambda^2}, \quad \lambda = 1, \dots, 3N-3. \quad (4.6)$$

Hence $\langle d(t) \rangle$ contains the -2 moment of the frequency distribution, $\langle \omega^{-2} \rangle$ as defined in Eq. (3.2), and this can be expressed in terms of the characteristic temperature Θ_{-2} , from Eq. (3.4), to yield the final result

$$\langle d(t) \rangle = \frac{3\hbar^2 T}{M k_B \Theta_{-2}^2}. \quad (4.7)$$

To make a systematic study of nondiffusing states, we brought the system to equilibrium states on the random, symmetric, and bcc branches, using both heating and cooling procedures. As noted in Sec. II, the random states are long lived for $T \lesssim 35$ K. Since the random valleys have a universal harmonic shape, and, in particular, a universal value for Θ_{-2} , then all random valleys should conform to a single theoretical expression for D_I , namely, that given by Eq. (4.7) with $\Theta_{-2} = 114$ K. Inserting the numbers gives for random valleys

$$D_I(a_0^2) = 0.00174T(\text{K}). \quad (4.8)$$

Figure 12 shows our MD results for D_I , evaluated from the $d(t)$ curves in Fig. 11(a), and additional such curves, for random states at temperatures up to 35 K. The data of Fig. 12 are obtained from two different random valleys, for $N = 500$ and 1000, and hence further demonstrate the uniformity of different random valleys in their macroscopic prop-

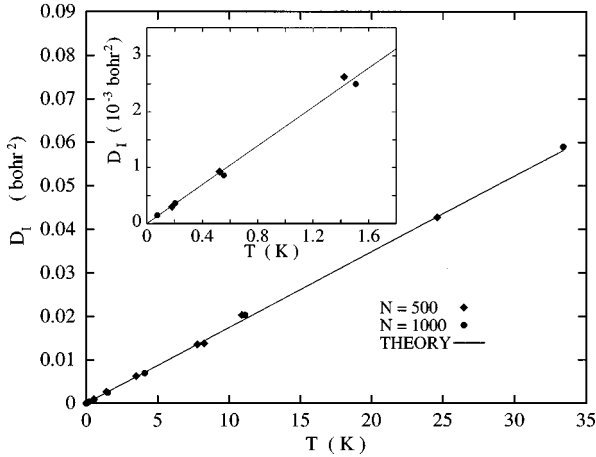


FIG. 12. Intercepts D_I for nondiffusing random states. The theoretical curve labeled THEORY is the harmonic approximation given by Eq. (4.8). The inset shows the highly linear behavior of D_I , and its good fit to the harmonic theory, in the small T regime.

erties. Notice that each point plotted in Fig. 12 represents a separate random state, hence each point is independent confirmation of the theoretical expression, Eq. (4.7) or (4.8). From the graph of Fig. 12, there can be no doubt that, for every nondiffusing random state we studied, the system is moving entirely within a single nearly harmonic random valley.

Again as noted in Sec. II(b), random states above 35 K generally live long enough to obtain respectable MD data. We examined such states at temperatures up to 88 K, and found the same behavior as described above, but with larger scatter in the results, namely, $D_M=0$, and D_I agrees with the theoretical single-harmonic valley expression [Eq. (4.7) or (4.8)].

For the bcc valley, Eq. (3.13) lists $\Theta_{-2}=121.4$ K, and this together with Eq. (4.7) gives the harmonic result

$$D_I(a_0^2)=0.001\,534T \text{ (K)}. \quad (4.9)$$

Graphs of $d(t)$ for the bcc states, similar to the ones shown in Fig. 11, have $D_M=0$, and yield the set of D_I plotted in Fig. 13. These values of D_I are in excellent agreement with Eq. (4.9) at low temperatures, and the slight drift of D_I below Eq. (4.9) at higher temperatures is presumably a result of anharmonicity.

We also made a series of calculations for a single symmetric valley that has $\Theta_{-2}=118$ K. Up to 212 K, the graphs of $d(t)$ have $D_M=0$. Here again the values of D_I obtained from $d(t)$ are in excellent agreement with the single-harmonic valley equation, Eq. (4.7), as shown in Fig. 13, where the theoretical curve is

$$D_I(a_0^2)=0.001\,62T \text{ (K)}. \quad (4.10)$$

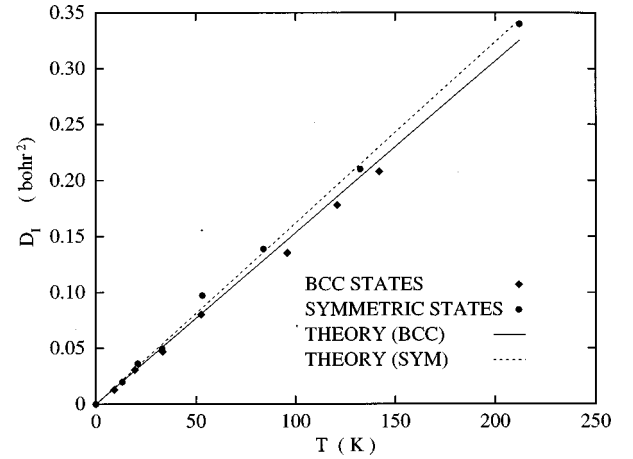


FIG. 13. Same as Fig. 12 but for nondiffusing bcc and symmetric states. The theoretical curves labeled THEORY (BCC) and THEORY (SYM) are the single-valley harmonic approximation for bcc [Eq. (4.9)], and for a single symmetric valley [Eq. (4.10)].

Our conclusion at this point is that for every state having $D_M=0$, random, symmetric, or crystalline, the system moves within a single nearly harmonic potential valley.

V. SUMMARY OF CONCLUSIONS

We have used MD calculations to probe that part of the many-particle potential surface that is visited by the monatomic liquid. We have used techniques of cooling and heating the system, and MD runs to establish equilibrium. Our calculations were done for a system that is an accurate representation of metallic sodium, at the density of the liquid at melt, and with $N=432$ for bcc states, and $N=500, 1000$, and 3000 for noncrystalline states. Our conclusions are organized into five major points, as follows.

(1) The potential surface is composed of a large number of stable nearly harmonic valleys. We should emphasize that every valley we examined, without exception, was found to be both stable and approximately harmonic. Stability is shown, to numerical accuracy, by finding that the system freezes to a configuration that is permanent under continued quenching and MD runs. The nearly harmonic character of the valleys is indicated by two observed properties. First, that the slope of $\langle \Phi/N \rangle$ versus $\langle K/N \rangle$ is approximately unity for the random states, the symmetric states, and the bcc states, as shown in Fig. 3, strongly suggests that the system moves among nearly harmonic valleys in each of these groups of states. This same property of the liquid states, expressed in the form that the ion motional specific heat is approximately $3k_B$ per atom, was taken as evidence of nearly harmonic valleys in our original formulation of liquid dynamics [1]. Second, when the system is moving within a single valley, as indicated by the property $D_M=0$, the time average of the mean square displacement is in accurate agreement with harmonic theory, Eq. (4.7), and this is strong evidence that the particular valley in question is nearly harmonic. Figure 12 shows this property for random valleys to 35 K, and the same result holds with a little more scatter (because the states are short lived) to approximately 100 K. Figure 13 shows the nearly harmonic property for the bcc valley to 143 K, and for

a single symmetric valley to 212 K.

(2) Stable valleys have previously been observed in computer simulations, and have been classified as crystalline or amorphous [3–10]. Here we find the amorphous class is further subdivided into two groups, which we call random and symmetric. To express the properties of these valleys, we recall Eqs. (3.8)–(3.11), where the potential surface is expanded about the minimum of a given valley, in the form $\Phi = \Phi_0 + \Phi_H + \Phi_A$. Φ_0 is the potential at equilibrium (at the structure), Φ_H is the harmonic potential, of second order in displacements from equilibrium, and diagonalized to a sum of squares of normal coordinates, and Φ_A is the anharmonic potential. An important measure of Φ_H is the spectrum of its eigenvalues, and three key moments of this spectrum are contained in the three characteristic temperatures $\Theta_n, n = -2, 0, 2$, which we studied extensively.

The important properties of the random valleys are listed in three statements. First, they are macroscopically uniform, i.e., they all have virtually the same value of Φ_0 , virtually the same eigenvalue spectrum of Φ_H , and they all have small anharmonicity. Second, on the microscopic level, Φ_A has a contribution that is irregular at very small scale, and that differs from one random valley to another. Third, the random valleys cover by far the major portion of configuration space, hence they dominate the statistical mechanics of the liquid state.

The important properties of symmetric valleys are most conveniently listed by making comparisons with the random valleys. First, the symmetric valleys lie at lower potential, i.e., they have a lower value of Φ_0 , as shown in Fig. 3, and they are not macroscopically uniform, but instead have a noticeable scatter in their potential parameters Φ_0 and Θ_n . These properties presumably result from some remnant of crystalline symmetry, present in symmetric valleys but not in random ones. Second, on the microscopic level, Φ_A in symmetric valleys also has a contribution which is irregular at a very small scale. Third, the symmetric valleys cover a relatively small portion of configuration space, hence they do not contribute to the statistical mechanics of the liquid state.

(3) The equilibrium states of our system, from zero temperature up to and including the liquid states, conform to the above description of the potential surface. We make the following interpretation of the observed motion of our system.

For $T \lesssim 35$ K, random states are long lived, and in each random state $D_M = 0$, and the system moves within a single random valley. The system has not enough energy to get over the lowest ridge enclosing its valley within the time of our MD run. We presume the system *would* get out of its random valley, if we could continue the MD run for a sufficient (*very* long) time.

For $35 \text{ K} \lesssim T \lesssim 100$ K, random states are short-lived states and decay into symmetric states, though while the system is in a random state it shows $D_M = 0$, and it appears to move within a single random valley. In fact, we presume the system is actually moving from one random valley to another, but at such a slow rate that the motion cannot be distinguished in our MD data, until the system arrives at a symmetric valley, where it loses potential energy and becomes trapped.

For $100 \text{ K} \lesssim T \lesssim 200$ K, random states are short lived and decay into symmetric states, and while the system is in a

random state it shows D_M small but nonzero, indicating the system is moving among random valleys. The system continues this motion until it encounters a symmetric valley, where it loses potential energy and becomes trapped.

For $T \gtrsim 200$ K, random states are long lived and show substantial diffusion (large D_M). We presume the system is moving rapidly among potential valleys, both random and symmetric, and the system has sufficient energy that it cannot become trapped in a symmetric valley. This description includes the liquid states at $T > 371$ K.

For $0 \text{ K} \lesssim T \lesssim 200$ K, symmetric states are long lived, and in each symmetric state $D_M = 0$, and the system moves within a single symmetric valley. Some irregular movement among valleys, which we have not yet analyzed, takes place in symmetric states above 200 K.

In bcc states, $D_M = 0$ and the system moves within a single bcc valley. This was verified by our MD calculations to 143 K, and presumably continues to hold to approximately 350 K.

(4) In order to construct liquid dynamics theory, in such a form that the partition function and free energy could actually be evaluated, it was necessary to make a simple but physically realistic model of the many-particle potential surface [1]. The above description of the potential surface, resulting from the present extensive computer calculations, confirms the simple liquid-dynamics model in excruciating detail. This means further that the universal-random-valley potential parameters, specifically Φ_0 and Θ_n for $n = -2, 0, 2$, as calculated here for metallic sodium at the density of the liquid at melt, are the essential parameters for the liquid-dynamics theory of sodium at that density. We could imagine that this same procedure will be successful in evaluating the liquid-dynamic parameters for other elements as well.

(5) The present calculations allow us to test two predictions of liquid-dynamics theory [1]. The first prediction, based strongly on the universality of the constant-volume entropy of melting for normal melting elements, is that the characteristic temperature Θ_0 for the crystal, and for the random valleys, should be nearly the same at the same density, say, within 5%. Here we find $\Theta_0(\text{bcc}) = 99.65$ K, and $\Theta_0(\text{random}) = 98.7$ K, in remarkable confirmation of the prediction.

The second prediction, based on approximating both crystal and random valleys as purely harmonic, is that Φ_0 for random valleys should lie above Φ_0 for the crystal at the same density, by the amount $T_m \Delta S$, where ΔS is the constant-volume entropy of melting. Experiment for sodium gives $T_m \Delta S = 1.7$ mRy/atom at density of the liquid at melt [23]. On the other hand, from our present calculations (see Fig. 3), Φ_0 (random) lies above Φ_0 (bcc) by 0.92 mRy/atom. The sizable error of the liquid-dynamics prediction is due to the anharmonicity of the random states, as revealed in the graph of $\langle \Phi/N \rangle$ versus T in Fig. 4. It remains to be learned whether such large anharmonicity is usual or exceptional among the elements.

ACKNOWLEDGMENT

This work was supported, in part, by the Department of Energy under Contract No. W-7405-ENG-36.

- [1] D.C. Wallace, Phys. Rev. E **56**, 4179 (1997).
- [2] D.C. Wallace, Phys. Rev. E **56**, 1981 (1997).
- [3] F.H. Stillinger and T.A. Weber, Kinam **3**, 159 (1981).
- [4] F.H. Stillinger and T.A. Weber, Phys. Rev. A **25**, 978 (1982).
- [5] F.H. Stillinger and T.A. Weber, Phys. Rev. A **28**, 2408 (1983).
- [6] T.A. Weber and F.H. Stillinger, J. Chem. Phys. **80**, 2742 (1984).
- [7] F.H. Stillinger and T.A. Weber, Science **225**, 983 (1984).
- [8] R.A. LaViolette and D.M. Stump, Phys. Rev. B **50**, 5988 (1994).
- [9] A. Rahman, M.J. Mandell, and J.P. McTague, J. Chem. Phys. **64**, 1564 (1976).
- [10] R.A. LaViolette and F.H. Stillinger, J. Chem. Phys. **83**, 4079 (1985).
- [11] W. A. Harrison, *Pseudopotentials in the Theory of Metals* (Benjamin, New York, 1972).
- [12] D. C. Wallace, *Thermodynamics of Crystals* (Dover, New York, 1998).
- [13] D.C. Wallace, Phys. Rev. **176**, 832 (1968).
- [14] R.E. Swanson, G.K. Straub, B.L. Holian, and D.C. Wallace, Phys. Rev. B **25**, 7807 (1982).
- [15] S.K. Schiferl and D.C. Wallace, Phys. Rev. B **31**, 7662 (1985).
- [16] G.K. Straub, S.K. Schiferl, and D.C. Wallace, Phys. Rev. B **28**, 312 (1983).
- [17] G.K. Straub and D.C. Wallace, Phys. Rev. B **30**, 3929 (1984).
- [18] B.L. Holian, G.K. Straub, R.E. Swanson, and D.C. Wallace, Phys. Rev. B **27**, 2873 (1983).
- [19] M. P. Allen and D. J. Tildesley, *Computer Simulation of Liquids* (Oxford University Press, Oxford, 1990).
- [20] R.D. Mountain and P.K. Basu, J. Chem. Phys. **78**, 7318 (1983).
- [21] J. P. Hansen and I. R. McDonald, *Theory of Simple Liquids*, 2nd ed. (Academic, New York, 1986).
- [22] S.J. Larsson, C. Roxbergh, and A. Lodding, Phys. Chem. Liq. **3**, 137 (1972).
- [23] D.C. Wallace, Proc. R. Soc. London, Ser. A **433**, 631 (1991).